Optomagnonic Whispering Gallery Microresonators

Xufeng Zhang,[1] Na Zhu,[1] Chang-Ling Zou,[1,2] and Hong X. Tang[1,*]

[1]*Department of Electrical Engineering, Yale University, New Haven, Connecticut 06511, USA*
[2]*Department of Applied Physics, Yale University, New Haven, Connecticut 06511, USA*
(Received 13 October 2015; published 16 September 2016)

Magnons in ferrimagnetic insulators such as yttrium iron garnet (YIG) have recently emerged as promising candidates for coherent information processing in microwave circuits. Here we demonstrate optical whispering gallery modes of a YIG sphere interrogated by a silicon nitride photonic waveguide, with quality factors approaching 10^6 in the telecom *c* band after surface treatments. Moreover, in contrast to conventional Faraday setups, this implement allows an input photon polarized colinearly to the magnetization to be scattered to a sideband mode of orthogonal polarization. This Brillouin scattering process is enhanced through triply resonant magnon, pump, and signal photon modes within an "optomagnonic cavity." Our results show the potential use of magnons for mediating microwave-to-optical carrier conversion.

Hybrid magnonic systems have been emerging recently as an important approach towards coherent information processing [1–9]. The building block of such systems, the magnon, is the quantized magnetization excitation in magnetic materials [10,11]. Its great tunability and long lifetime make the magnon an ideal information carrier. Particularly, in a magnetic insulator yttrium iron garnet (YIG), magnons interact with microwave photons through magnetic dipole interaction, which can reach the strong and even ultrastrong coupling regime thanks to the large spin density in YIG [4–6]. Besides, magnons can also couple with elastic waves [12,13] and optical lights [14,15], so they are of great potential as an information transducer that mediates interconversion among microwave photons, optical photons, and acoustic phonons. Long desired functions, such as microwave-to-optical conversion, can be realized on such a versatile platform.

Magneto-optical (MO) effects such as the Faraday effect have been long discovered and utilized in discrete optical device applications [16–18]. Based on such effects, magnons can coherently interact with optical photons. On the one hand, magnons can be generated by optical pumps [19–22], while on the other hand, optical photons can be used to probe magnons through Brillouin light scattering [15,23]. However, in previous studies the typical geometries are all thin film or bulk samples inside which optical photons interact with magnons very weakly and usually through only a single pass. For high-efficiency magnon-photon interaction, it is desirable to obtain triple-resonance condition of high quality (Q) factor modes, i.e., to have the magnons as well as the input and output optical photons simultaneously on resonance.

In this Letter, we demonstrate the magnon-photon interaction in a high-Q optomagnonic cavity that simultaneously supports whispering gallery modes (WGMs) of optical and magnon resonances. With high-precision fabrication and careful surface treatment, the widely used YIG sphere structure, which is inherently an excellent magnonic resonator, exhibits high optical Q factors in our measurements. YIG has a high refractive index (2.2 in the telecom *c* band), which poses a challenge for efficient light coupling with tapered silica fibers due to index mismatch [24,25]. By employing an integrated optical waveguide fabricated on a silicon nitride substrate that has a similar refractive index (around 2.0) as YIG, we can efficiently couple to both the transverse-magnetic (TM) and transverse-electric (TE) optical resonances in the YIG sphere. We demonstrate that these optical WGMs, which were previously considered as in linear polarizations, can have Faraday effect and therefore interact with magnons thanks to their effective circular polarization [26–28]. Moreover, the cavity enhancement for both the pumping and scattered photons drastically boosts up the magnon-photon interaction. Further device scaling and improvements allow the coupled system to enter the regime where magnons can be coherently converted into optical photons. Our results demonstrate that the YIG sphere is a very promising platform to bridge the gap between magnons and optical photons, which not only moves the hybrid magnonic system design into the optical regime but also paves the way towards using the magnon as a transducer for coherent information processing between carriers that are orders of magnitude different in frequencies.

In magnetized YIG materials, magnons are the collective excitations of spin states of Fe^{3+} ions [29]. The creation or annihilation of a single magnon corresponds to the ground spin flip. At microwave frequencies, the magnon state can be manipulated straightforwardly by magnetic dipolar transition using the oscillating magnetic fields of microwave photons. While at optical frequencies, magnon

manipulation becomes difficult because the magnetic transition is negligible while direct spin flip by electric dipolar transition is forbidden [30]. Alternatively, optical photons can modify ground state spins through a two-photon transition by means of an orbital transition and the spin-orbit interaction (the MO effect) [14]. Such a process has been previously studied using conventional Faraday setups [31], in which light propagates parallel to the magnetic field and interacts with magnons in a single pass. It is natural to consider shaping the YIG into an optical cavity where light passes the magnetic material multiple times to boost up the magnon-photon interaction. Therefore, we propose using a whispering gallery resonator made of YIG to provide enhanced magnon-photon coupling in a triply resonant configuration, and the mechanism is explained in the following discussions.

The optomagnonic cavity we used in our experiments is a single crystal YIG sphere. Because of the spherical symmetry, lights are confined in the sphere by total internal reflection and form WGMs. Each optical WGM is characterized by three mode numbers (q, l, n), which correspond to the radial, angular, and azimuthal order $(n = -l, ..., l)$, respectively [32,33]. Moreover, the WGMs are also characterized by their polarization, i.e., the direction of their electric field distribution. Conventional Faraday setups require the bias magnetic field to be parallel to the direction of light propagation. However, for WGMs the light propagates along the circumference of the sphere [Fig. 1(a)], and therefore the bias magnetic field should be in the x-y plane. Because of the geometry symmetry, the MO effect vanishes for such a Faraday configuration. At first glance, the MO effect also vanishes when the bias magnetic field is along the z direction, since it requires circular polarization in respect to $\vec{H}$ while WGMs are linearly polarized, with electric fields either parallel (TM) or perpendicular (TE) to the z direction. However, thanks to the field gradient at the dielectric interface [26–28], there exist nonzero optical electric fields along the propagation direction for the TE polarized WGMs. As a result, the electric field rotates within the x-y plane and forms a cycloid trajectory, similar to the elliptically polarized light propagating in the free space. Therefore, the TE WGMs possess partial circular polarization (σ^+) and can have magnetic response via the Faraday effect, as schematically illustrated in Fig. 1(a). Note that the pump light can propagate either clockwise (CW) or counterclockwise (CCW), and accordingly the conservation conditions are different when interacting with magnons, as is shown below.

Similar to the optical WGMs, magnon modes in the YIG sphere can also be characterized by three mode numbers (q_m, l_m, n_m) [34]. For the uniform magnon mode (all the spins precessing in phase) whose frequency is determined by $\omega_m = \gamma H$ (where $\gamma = 2\pi \times 2.8$ MHz/Oe is the gyromagnetic ratio and H is the external bias magnetic field) [5], the corresponding mode numbers are $(1,1,1)$. The microscopic mechanism of the magnon-photon interaction is intrinsically a three-wave process, as schematically
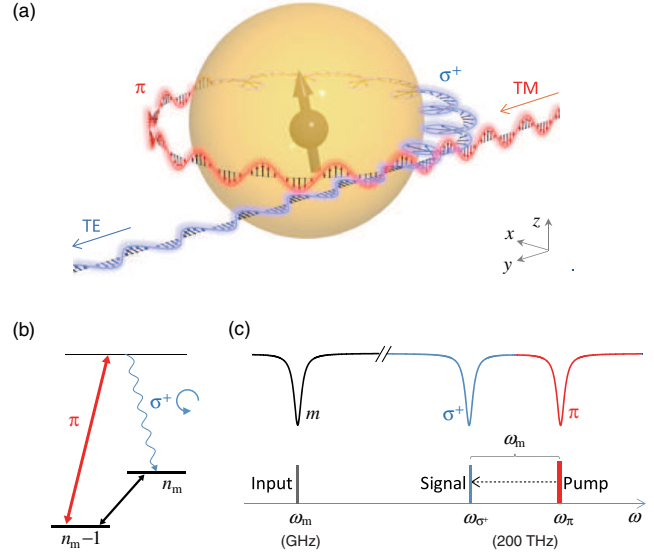

FIG. 1. (a) Schematic illustration of the magnon-photon interaction. The YIG sphere is biased by a magnetic field along the z direction, while the WGMs propagate along the perimeter in the x-y plane. The TM input light excites the π WGM in the YIG sphere, which is scattered by the magnon into a σ^+ polarized photon and then converts to the TE output in the waveguide. (b) Energy level diagram of the magnon-photon interaction. (c) Triple-resonance condition for the enhanced magnon-photon interaction process in the optomagnonic resonator. m represents the magnon resonance (at frequency ω_m). σ^+ and π represent the two optical resonances with orthogonal polarizations (at frequency ω_{σ^+} and ω_π, respectively).

illustrated by Fig. 1(b). Because of the spin angular momentum conservation, every time the magnon number increases by 1, it indicates that the electron spin increases by 1, which corresponds to a two-photon transition in the form of $\sigma^- \to \pi$ (CCW) or $\pi \to \sigma^+$ (CW). As a result, there is only one optical sideband generated for a given pumping light direction. The mesoscopic model of the MO effect is represented by the permittivity tensor $\varepsilon_{ij} = \varepsilon_0(\varepsilon_r \delta_{ij} - if\epsilon_{ijk}M_k)$ [29], where ε_0 is the vacuum permittivity, ε_r is the relative permittivity of YIG, δ_{ij} and ϵ_{ijk} are Kronecker and Levi-Civita symbols, f is the Faraday coefficient, M_k is the magnetization, and i, j, k correspond to the x, y, z direction, respectively. When the energy is conserved for the two-photon and magnon transitions in which $\omega_1 - \omega_2 = \omega_m$, the coupling strength between two optical modes is $g = \int \Delta\varepsilon_{ij}(\vec{x})E_{1,i}^*(\vec{x})E_{2,j}(\vec{x})d\vec{x}^3$, where $E_{p,i}(\vec{x})$ $(p = 1, 2)$ is the normalized field of the optical WGM $\int \varepsilon_{ii}(\vec{x})|E_{p,i}(\vec{x})|^2 d\vec{x}^3 = \omega_p$, and the magnon induced permittivity change is $\Delta\varepsilon_{ij}(\vec{x}) = -if\varepsilon_0\epsilon_{ijk}M_k(\vec{x})$. As the field distributions are in the form of $e^{in\phi}$ in the spherical coordinate along the azimuthal direction, g is nonzero only for the conservation of orbit angular momentum $n_1 - n_2 = n_m$. Therefore, when the energy, spin, and orbit angular momentum conservation relations, i.e., the triple-resonance condition [Fig. 1(c)] and selection rule for our optomagnonic resonator, are simultaneously satisfied, the coupling strength g can be greatly enhanced.
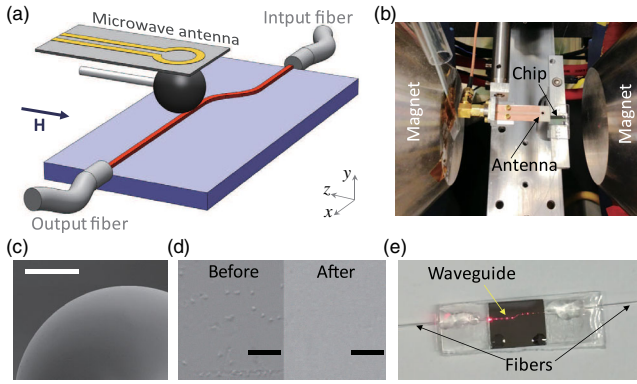
FIG. 2. [(a) and (b)] Schematic and optical image of the experimental assembly of our optomagnonic device, respectively. (c) Scanning electron microscope image of the polished YIG sphere. The scale bar is 100 μm. (d) The surface of the YIG sphere before and after our surface treatment process. Scale bars are 1 μm. The submicrometer particles vanish after the surface treatment. (e) Optical image of the silicon nitride coupling waveguide chip with glued fibers on the two sides. The chip and the fibers are attached to a piece of glass holder for mechanical support and to reduce long-term drift.

The schematic and optical images of the experiment assembly of our optomagnonic cavity integrated with photonic and microwave circuits are shown in Figs. 2(a) and 2(b), respectively. A 300-μm-diameter single crystal YIG sphere [Fig. 2(c)] is glued to a 125-μm-diameter supporting silica fiber. Although YIG spheres have been widely used as magnon resonators, their potential as high-Q optical WGM microresonators has been overlooked. In fact, the low absorption loss of YIG in infrared wavelengths (0.13 dB/cm) [35] can lead to Q factors as high as 3×10^6. Nevertheless, the surface defects and contaminations of commercial YIG sphere products induce strong scattering losses, limiting the highest achievable Q factor in our experiment. A major contribution of the surface contamination is the residual of the submicrometer aluminum oxide polishing grit used in the YIG sphere production process, which is very difficult to remove using conventional cleaning procedures. By combining a mechanical polishing procedure (using silicon oxide slurry) and a follow-up chemical cleaning procedure (using buffered oxide etch), we efficiently removed these contaminations and obtained very clean sphere surfaces [Fig. 2(d)]. To excite high-Q WGMs, the conventional tapered silica fiber (effective refractive index around 1.16 for a 1-μm-diameter tapered fiber) approach cannot achieve high efficiency because of the index mismatch [24,25]. Therefore, we integrated the YIG sphere with a silicon nitride optical circuit [Fig. 2(e)], which supports waveguide modes that have much smaller index mismatch (effective refractive index is 1.65 for the fundamental TM mode and 1.50 for the fundamental TE mode in a 3.8-μm-wide, 330-nm-thick waveguide) with the YIG sphere WGMs thanks to its larger material index [36–38]. The photonic chip is glued to silica optical fibers
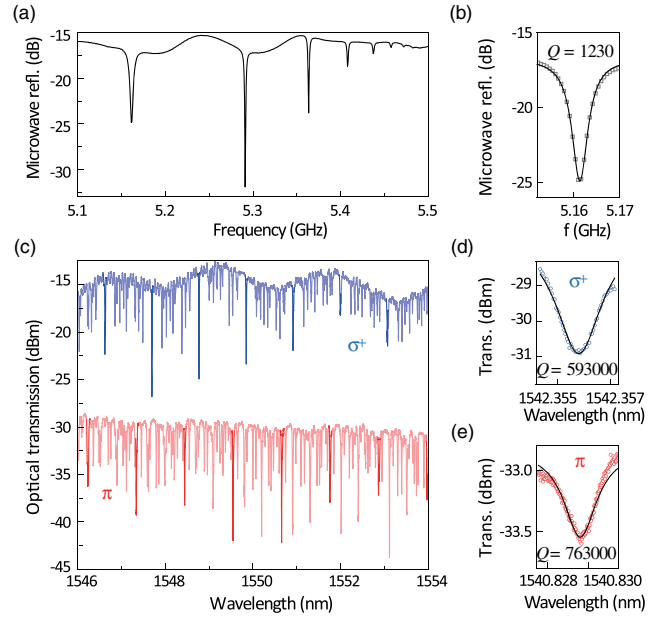

FIG. 3. (a) Magnon resonances measured on a 300-μm-diameter YIG sphere biased at 1840 Oe. (b) The zoomed-in spectrum of the fundamental magnon mode. (c) Optical WGMs for both polarizations (σ^+ and π) measured on the same YIG sphere using the silicon nitride coupling waveguide. The large extinction ratio and periodic mode distribution are evident. (d) and (e) are the zoomed-in spectrum for the two polarizations, respectively.

using UV curable epoxy after careful alignments, which provides high coupling efficiency and stable transmission. A coplanar loop antenna circuit is placed in the vicinity of the YIG sphere to convert the microwave signal to magnons. In our experiments, the YIG sphere is always biased by an external magnetic field along the supporting fiber (z) direction according to the spin conservation condition discussed above.

Before studying the magnon-photon interaction, we first characterize the optical and magnon modes. The reflection microwave spectrum at $H = 1840$ Oe is plotted in Fig. 3(a), showing multiple dips that correspond to magnon modes (to observe high order modes, the YIG sphere is placed at the nonuniform fields of the antenna). In the zoomed-in spectrum of Fig. 3(b), the loaded Q factor of the uniform magnon mode is 1230. In the following magnon-photon interaction measurement, the YIG sphere is placed at the uniform microwave fields of the antenna output such that only the uniform magnon mode is excited. The optical transmission spectra are plotted in Fig. 3(c), where TE/TM polarized light in the waveguide is used to probe σ^+/π polarized WGMs in the YIG sphere, receptively. Groups of optical resonances show up in the spectra, exhibiting large extinction ratios (beyond 10 dB) for both polarizations, which confirms the efficient coupling between the silicon nitride waveguide and the WGMs. The measured free spectral ranges for both the σ^+ (1.0765 nm) and π (1.1068 nm) polarization agree with the prediction (1.1580 nm) for WGMs. Thanks

to our surface treatments, very high optical Q factors are achieved: $Q_{\sigma^+} = 0.593 \times 10^6$ and $Q_\pi = 0.763 \times 10^6$ [Figs. 3(d) and 3(e)].

To measure the interaction between the optical photon and magnon, the YIG sphere is biased at $H = 2410$ Oe, corresponding to a magnon resonance frequency of $\omega_m/2\pi = 6.75$ GHz. The optomagnonic resonator is pumped by a TM polarized laser beam with 1 mW power, and the magnons are excited by an on-resonance microwave signal. The laser wavelength is scanned to search for the optical modes that satisfy the energy, spin, and angular momenta conservation conditions. During the searching process, the lock-in technique is adopted to improve the converted light signal to noise ratio [36]. When the conservation conditions are satisfied, the output light is sent to a high resolution spectrometer for further analysis. It is worth noting that the density of optical WGMs is very large, as there exists mode degeneracy in the polar direction and high order modes in the radial direction. As a result, the conservation conditions can be satisfied accidentally, similar to the Brillouin scattering in microsphere optomechanical cavities [39,40]. A typical spectrum of converted photons as a function of the sweeping pump laser wavelength is shown in Fig. 4(a), where the passive transmission spectrum of the pump light is also shown accordingly. The correspondence between the resonances for pump light and the peaks of magnon-photon conversion implies the triple-resonance enhancement in our optomagnonic cavity. The dependence of the converted photons on the microwave resonance [Fig. 4(b)] also confirms the participation of the magnon in the inelastic light scattering process.

The detailed spectrum for one selected triple-resonance condition is plotted in Fig. 4(c), where the optomagnonic resonator is pumped by a TM light at 1534.599 nm. A polarization beam splitter is used to separate the two polarizations. The TM component of the output light shows a single peak as it only contains the transmitted pump light. On the contrary, the TE component shows two peaks: a strong peak that corresponds to the transmitted pump light that is not completely filtered out, and a weak sideband that corresponds to the generated photons. Therefore, we do have orthogonal polarizations for the generated signal and the pump light, which agrees well with our theory model. The linewidths of the measured pump and sideband signals are not the physical linewidth of the light but instead only represent the finite resolution (67 MHz) of the filter in the spectrometer. The centers of the pump peak and sideband differ from each other by 6.75 GHz, matching the input magnon frequency. The sideband appears only on one side of the pump as a result of the conservation conditions, as explained in the above analysis.

We measured the converted light at various microwave input powers, which clearly shows a linear power dependence [Fig. 4(d)], indicating a linear magnon-to-photon conversion. The fitted raw power (system) conversion efficiency is 5×10^{-8}, corresponding to a microwave-to-optical photon number ratio of 1.7×10^{-12}. An internal power conversion efficiency can be estimated as 6×10^{-3}
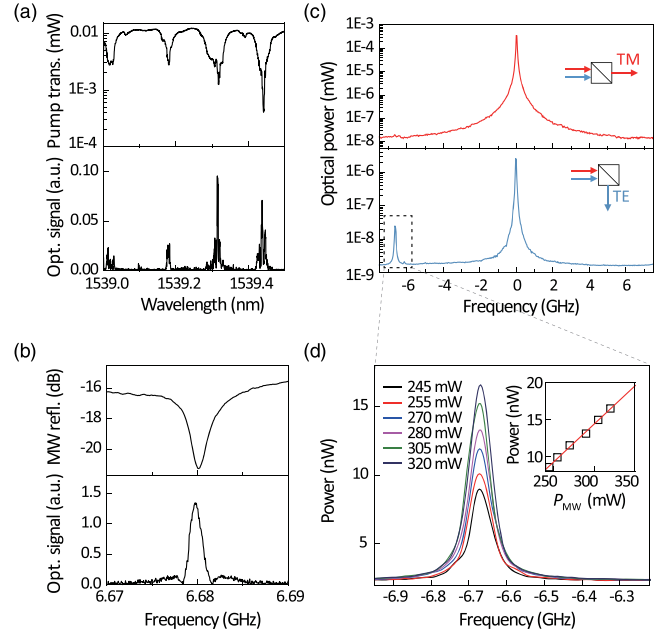

FIG. 4. (a) Optical pump transmission and the generated optical signal as a function of pump laser wavelength. The correspondence of the generated optical signal peak and the optical pump resonance dip indicates the satisfaction of the conservation conditions. (b) Microwave reflection and the generated optical signal as a function of the microwave frequency. (c) Optical spectrum of the device output when the triple-resonance condition is satisfied. The TM and TE components of the output light are separated by a polarization beam splitter. The TM component corresponds to the direct transmission of the pump light, while the TE component contains the scattered sideband. (d) Power dependence of the sideband on the input microwave power P_{MW}. Inset: extracted sideband power as a function of the input microwave power.

after taking various insertion losses into consideration (microwave insertion loss, 11 dB; single side chip insertion loss, 27 dB; sphere-waveguide coupling, 3 dB; insertion loss from fiber link after the chip, 10 dB), which corresponds to a magnon-to-optical photon number ratio of 2×10^{-7}. From the measurement results, the intrinsic magnon-photon coupling strength can be estimated [36] as $g/2\pi = 10.4$ Hz. With 30 μW optical power to the device (in the waveguide), the coupling strength is enhanced to $G/2\pi = 73$ kHz, corresponding to a cooperativity $C = G^2/(\kappa_m \times \kappa_o) = 5.4 \times 10^{-7}$ (κ_o is the dissipation rate of the WGMs) [36]. Currently, the conversion efficiency might be improved in several aspects: scaling down the sphere size to reduce the mode volumes of both magnon and optical fields in a similar way pacing up the state-of-the-art development in cavity optomechanics; engineering the cavity structure such as microrings to increase the overlap between optical and magnon fields; further improving the surface quality of the YIG sphere and purifying the YIG material; and doping YIG to obtain larger Faraday coefficients. With these improvements, it is possible to enhance the coupling strength to the $G/2\pi = 10$ MHz level [41]. This corresponds to an enhancement of

20000 for the cooperativity, and consequently the magnon-to-optical photon number ratio $\eta \propto [4C/(1+C)^2]$ can be boosted up to 0.4%. Such an efficiency makes the quantum-limited microwave-to-optical conversion feasible, which would overcome the inhomogeneous broadening problem encountered in the dilute rare-earth atom ensembles [42].

In conclusion, we have demonstrated an excellent optomagnonic resonator that is made by a highly polished YIG sphere. Utilizing an integrated optical chip for high-efficiency optical coupling, high-Q optical WGMs are observed in addition to magnon resonances in the YIG sphere after our careful surface treatment. When the triple-resonance condition and angular momentum conservation condition are satisfied, the magnon is converted to the optical photon with internal power efficiency of about 0.6%. This efficiency can be further improved by doping or geometry optimization. As the optical interface we used here is completely compatible and can be conveniently integrated with microwave systems [4–6] to obtain strong coupling between magnons and microwave photons, our results show the great potential of YIG spheres in designing complex hybrid systems towards realizing information interconversion among magnons, microwave photons, and optical photons.

---

[*]hong.tang@yale.edu

[1] A. V. Chumak, V. I. Vasyuchka, A. A. Serga, and B. Hillebrands, Nat. Phys. **11**, 453 (2015).
[2] Y. Tabuchi, S. Ishino, A. Noguchi, T. Ishikawa, R. Yamazaki, K. Usami, and Y. Nakamura, Science **349**, 405 (2015).
[3] C.-M. Hu, Phys. Canada **72**, 76 (2016).
[4] Y. Tabuchi, S. Ishino, T. Ishikawa, R. Yamazaki, K. Usami, and Y. Nakamura, Phys. Rev. Lett. **113**, 083603 (2014).
[5] X. Zhang, C.-L. Zou, L. Jiang, and H. X. Tang, Phys. Rev. Lett. **113**, 156401 (2014).
[6] M. Goryachev, W. G. Farr, D. L. Creedon, Y. Fan, M. Kostylev, and M. E. Tobar, Phys. Rev. Applied **2**, 054002 (2014).
[7] L. Bai, M. Harder, Y. P. Chen, X. Fan, J. Q. Xiao, and C.-M. Hu, Phys. Rev. Lett. **114**, 227201 (2015).
[8] H. Huebl, C. W. Zollitsch, J. Lotze, F. Hocke, M. Greifenstein, A. Marx, R. Gross, and S. T. B. Goennenwein, Phys. Rev. Lett. **111**, 127003 (2013).
[9] X. Zhang, C.-L. Zou, N. Zhu, F. Marquardt, L. Jiang, and H. X. Tang, Nat. Commun. **6**, 8914 (2015).
[10] A. A. Serga, A. V. Chumak, and B. Hillebrands, J. Phys. D **43**, 264002 (2010).
[11] B. Lenk, H. Ulrichs, F. Garbs, and M. Münzenberg, Phys. Rep. **507**, 107 (2011).
[12] C. Kittel, Phys. Rev. **110**, 836 (1958).
[13] K. Sinha and U. Upadhyaya, Phys. Rev. **127**, 432 (1962).
[14] Y. Shen and N. Bloembergen, Phys. Rev. **143**, 372 (1966).
[15] S. Demokritov, B. Hillebrands, and A. Slavin, Phys. Rep. **348**, 441 (2001).
[16] M. Freiser, IEEE Trans. Magn. **4**, 152 (1968).
[17] *Magneto-Optics*, edited by S. Sugano and N. Kojima (Springer, Boston, 1999).
[18] L. Bi, J. Hu, P. Jiang, D. H. Kim, G. F. Dionne, L. C. Kimerling, and C. A. Ross, Nat. Photonics **5**, 758 (2011).
[19] A. Kirilyuk, A. V. Kimel, and T. Rasing, Rev. Mod. Phys. **82**, 2731 (2010).
[20] A. V. Kimel, A. Kirilyuk, P. A. Usachev, R. V. Pisarev, A. M. Balbashov, and T. Rasing, Nature (London) **435**, 655 (2005).
[21] T. Satoh, Y. Terui, R. Moriya, B. A. Ivanov, K. Ando, and E. Saitoh, Nat. Photonics **6**, 662 (2012).
[22] J. V. der Ziel, P. Pershan, and L. Malmstrom, Phys. Rev. Lett. **15**, 190 (1965).
[23] P. A. Fleury and R. Loudon, Phys. Rev. **166**, 514 (1968).
[24] C.-L. Zou, Y. Yang, C.-H. Dong, Y.-F. Xiao, X.-W. Wu, Z.-F. Han, and G.-C. Guo, J. Opt. Soc. Am. B **25**, 1895 (2008).
[25] Y. Liu, T. Chang, and A. E. Craig, Opt. Eng. (Bellingham, Wash.) **44**, 084601 (2005).
[26] C. Junge, D. O'Shea, J. Volz, and A. Rauschenbeutel, Phys. Rev. Lett. **110**, 213604 (2013).
[27] J. Petersen, J. Volz, and A. Rauschenbeutel, Science **346**, 67 (2014).
[28] I. Shomroni, S. Rosenblum, Y. Lovsky, O. Bechler, G. Guendelman, and B. Dayan, Science **345**, 903 (2014).
[29] D. D. Stancil and A. Prabhakar, *Spin Waves—Theory and Applications* (Springer, Boston, 2009).
[30] H. Le Gall, J. Phys. (Paris), Colloq. **32**, C1 (1971).
[31] A. Borovik-Romanov and N. Kreines, Phys. Rep. **81**, 351 (1982).
[32] V. B. Braginsky, M. L. Gorodetsky, and V. S. Ilchenko, Phys. Lett. **137A**, 393 (1989).
[33] A. Chiasera, Y. Dumeige, P. Féron, M. Ferrari, Y. Jestin, G. Nunzi Conti, S. Pelli, S. Soria, and G. C. Righini, Laser Photonics Rev. **4**, 457 (2010).
[34] P. Röchmann and H. Dösch, Phys. Status Solidi **82**, 11 (1977).
[35] D. L. Wood and J. P. Remeika, J. Appl. Phys. **38**, 1038 (1967).
[36] See Supplemental Material at http://link.aps.org/supplemental/10.1103/PhysRevLett.117.123605 for more details on experimental measurements and theoretical analysis.
[37] J. Levy, Ph.D. thesis, Cornell University, 2011.
[38] C. Krückel, Ph.D. thesis, Chalmers University of Technology, 2015.
[39] C.-H. Dong, Z. Shen, C.-L. Zou, Y.-L. Zhang, W. Fu, and G.-C. Guo, Nat. Commun. **6**, 6193 (2015).
[40] J. Kim, M. C. Kuzyk, K. Han, H. Wang, and G. Bahl, Nat. Phys. **11**, 275 (2015).
[41] T. Liu, X. Zhang, H. X. Tang, and M. E. Flatté, Phys. Rev. B **94**, 060405(R) (2016).
[42] L. A. Williamson, Y.-H. Chen, and J. J. Longdell, Phys. Rev. Lett. **113**, 203601 (2014).